Hindawi Publishing Corporation
Journal of Nanomaterials
Volume 2016, Article ID 8182190, 11 pages
http://dx.doi.org/10.1155/2016/8182190

Research Article

Synthesis of N/Fe Comodified TiO_2 Loaded on Bentonite for Enhanced Photocatalytic Activity under UV-Vis Light

Xi Cao,[1] Chen Liu,[2] Yandi Hu,[3] Wenli Yang,[3] and Jiawei Chen[1]

[1]*State Key Laboratory of Biogeology and Environmental Geology, China University of Geosciences, Beijing 100083, China*
[2]*Environmental Protection and Energy Saving Center, China Waterborne Transport Research Institute, Beijing 100088, China*
[3]*Department of Civil & Environmental Engineering, University of Houston, Houston, TX 77204-4003, USA*

Correspondence should be addressed to Jiawei Chen; chenjiawei@cugb.edu.cn

Received 7 December 2015; Accepted 21 January 2016

Academic Editor: Daniela Predoi

To improve the efficiency of TiO_2 as a photocatalyst for contaminant degradation, a novel nanocomposite catalyst of (N, Fe) modified TiO_2 nanoparticles loaded on bentonite (B-N/Fe-TiO_2) was successfully prepared for the first time by sol-gel method. The synthesized B-N/Fe-TiO_2 catalyst composites were characterized by multiple techniques, including scanning electron microscope (SEM), energy dispersive spectrometry (EDS), X-ray diffraction (XRD), Fourier transform infrared spectra (FT-IR), X-ray fluorescence (XRF), nitrogen adsorption/desorption, UV-Vis diffuse reflectance spectra (DRS), and electron paramagnetic resonance (EPR). The results showed that bentonite significantly enhanced the dispersion of TiO_2 nanoparticles and increased the specific surface area of the catalysts. Compared with nondoped TiO_2, single element doped TiO_2, or unloaded TiO_2 nanoparticles, B-N/Fe-TiO_2 had the highest absorption in UV-visible region. The photocatalytic activity of B-N/Fe-TiO_2 was also the highest, based on the degradation of methyl blue (MB) at room temperature under UV and visible light irradiation. In particular, the synthesized B-N/Fe-TiO_2 showed much greater photocatalytic efficiency than N/Fe-TiO_2 under visible light, the newly synthesized B-N/Fe-TiO_2 is going to significantly increase the photocatalytic efficiency of the catalyst using sun light.

1. Introduction

Environmental applications of titanium dioxide (TiO_2) have received a lot of recent interests from researchers. Due to its fine electronic properties, high photocatalytic activity, chemical stability, and low costs, TiO_2 is commonly used as a photocatalyst for the degradation of various pollutants [1, 2]. For the photocatalytic degradation, first, TiO_2 absorbs the solar light to boost its electrons from the valence band to the conduction band, thus forming electron-hole pairs (e^--h^+). Then, the holes, as oxidants on TiO_2 surface, can absorb H_2O and hydroxide ions and oxidize them to hydroxyl radicals, which are the main oxidizing agents for pollutant degradation [3, 4]. Despite the great potential of TiO_2 for environmental treatment, there are mainly three disadvantages that have impeded their large-scale application. First, due to its band structure, TiO_2 absorbs UV light which only accounts for 3–5% of sunlight [5]. Second, the high rate of electron-hole recombination in TiO_2 system leads to low photocatalytic efficiency [6]. Third, the fast agglomeration of TiO_2 nanoparticles causes the formation of larger particles resulting in lower catalytic efficiency [7]. To overcome these three difficulties, researchers have attempted to modify TiO_2 with three specific strategies.

First, doping design has been applied to extend the absorption band edge of TiO_2 from UV region to visible light region [8–12]. For example, TiO_2 has been doped with nitrogen, and the modified catalyst showed higher photocatalytic activity [13]. Regarding the mechanisms, Asahi suggested that N_{2p} level could mix with O_{2p}, which narrowed the band gap of the catalyst and extended its photocatalytic activity into the visible region [14, 15], while some other researchers suggested that N doping in TiO_2 (N-TiO_2) can create a midgap state serving as an electron acceptor or donor in the band gap of TiO_2, causing its increased photocatalytic activity under visible light [16–18].

Second, the photocatalytic efficiency also depends on the competition between the electron-hole recombination rate

and the surface charge carrier transfer rate. It was reported that small amount of Fe^{3+} ions can act as the traps for the photogenerated electrons and holes, resulting in the inhibition of electron-hole recombination. Therefore, Fe^{3+} has been doped in TiO_2 (Fe-TiO_2) to enhance the photocatalytic activity of TiO_2 [19–21].

Third, to prevent the agglomeration of TiO_2 nanoparticles, TiO_2 nanoparticles have been dispersed into the interlayers of clay minerals. Among the clay minerals, bentonite is widely used owing to economic concerns. The TiO_2 nanoparticles loaded on bentonite (B-TiO_2) showed increased specific surface area, thermal stability, cations exchange ability, and photocatalytic efficiency for pollutant degradation [22–25].

It is promising to combine the modification strategies for increasing the photocatalytic efficiency of TiO_2 nanoparticles. For example, TiO_2 nanoparticles have been comodified as N/Fe-TiO_2 (doped with both N and Fe) and B-Fe-TiO_2 (doped with Fe and loaded on bentonite), both of which showed improved photocatalytic activities compared to non-doped TiO_2, single element doped TiO_2, or unloaded TiO_2 nanoparticles [26–29]. A recent study synthesized that N/Fe-TiO_2 film on the bentonite surface by microwave power, loading TiO_2 nanoparticles on the bentonite surface by sol-gel method, has never been studied yet [30]. Sol-gel method serves as a common way to produce TiO_2 particles, since it has several advancements, such as producing nanosized crystallized powder of high purity at relatively low temperature, possibility of stoichiometry controlling process, and production of homogeneous materials [31]. Therefore, it is necessary to synthesize (Fe/N) comodified TiO_2 nanoparticles loaded on bentonite (B-N/Fe-TiO_2) by sol-gel method. Furthermore, there is no report on the B-N/Fe-TiO_2 photocatalytic efficiency difference under UV and visible lights for the degradation of a model pollutant methyl blue (MB). In this study, we synthesized and fully characterized B-N/Fe-TiO_2, and we measured its photocatalytic efficiency for MB degradation under UV and visible lights, and the mechanisms of its enhanced performance were also elucidated.

2. Experimental

2.1. Materials. Tetrabutyl titanate (TBOT), ethanol, and ferric chloride ($FeCl_3 \cdot 6H_2O$) were purchased from Sinopharm Chemical Reagents Company (China). Urea and acetic acid were purchased from Beijing Chemical Works. All the chemicals were of analytical grade and used without further purification. Type P25 TiO_2 was purchased from Evonik Degussa Company (Germany) with a grain size of 20 nm. Methyl blue (MB, reagent grade, Sinopharm Chemical Reagents Company) was selected as the probe compound for the photocatalytic degradation reactions. Na-bentonite was purchased from Sinopharm Chemical Reagents Company (China).

2.2. Synthesis of Modified TiO_2 Catalysts. Pure TiO_2 and modified TiO_2 were synthesized by a sol-gel process. First, an "A" solution was made by mixing 20 mL tetrabbutyl titanate, 60 mL absolute ethanol, and 2 mL acetic acid, while a "B" solution was made by mixing 0.6 mL HCl and 10 mL ultrapure water (18.3 MΩ cm). For the case of N and/or Fe modified TiO_2 synthesis, urea and/or ferric chloride were added to the "B" solutions. The molar ratio of Ti/N was 1 : 2 and the Fe ratio was 5 w%. Then, the modified "B" solution, containing urea and/or ferric chloride, was added dropwise to "A" solution under stirring vigorously, and pure TiO_2 and N and/or Fe modified TiO_2 were synthesized. For the synthesis of bentonite supported catalysts (B-TiO_2, B-N-TiO_2, B-Fe-TiO_2, and B-N/Fe-TiO_2), 1 g Na-bentonite was added into the mixtures of "A" and modified "B" solutions, and the solutions were stirred continuously for 2 hours. Finally, the solutions were let stand in room temperature for 12 hours, dried at 80°C for 24 hours, and calcined at 500°C for 3 hours with a heating rate of 5°C/min from room temperature. After synthesis, the calcined samples were ground and sieved, and fine powders smaller than 200 mesh size were used in the experiments.

2.3. Catalyst Characterization. Multiple techniques were employed to characterize the morphology, composition, and structure of the synthesized TiO_2 catalyst composites. The synthesized samples were coated with platinum, and their morphologies were observed using scanning electron microscopy (SEM, JSM-6460LV, Zeiss MERLIN VP Compact, Germany). The elemental compositions, in terms of weight and atomic percentages, of the catalyst composites were determined using energy dispersive spectrometry (EDS). In addition, the weight percentages of TiO_2 in the synthesized composites were measured by X-ray fluorescence spectrometry (XRF, XRF-1800, Japan). To characterize the structure of the catalyst composites, X-ray diffraction (XRD, Rigaku D/Max 2500, Japan) and Fourier transform infrared spectroscopy (FTIR, PerkinElmer) measurements were conducted.

Furthermore, specific properties (such as specific surface area, UV-Vis light absorption and $OH^{\bullet}$ and $O_2^{\bullet-}$ generation), which control the catalytic efficiency of the catalyst composites, were also characterized. The specific surface areas of the synthesized composites were measured using an Autosorb IQ2 nitrogen adsorption/desorption apparatus (Quantachrome, USA). The UV-Vis absorption spectra of the catalyst composites were measured by TU-1901 spectrophotometer. Electron paramagnetic resonance (EPR) spectra were acquired with a Bruker E580 CW spectrometer at 295 K, operating with a microwave frequency of 9.7 GHz. Both materials were weighted 15 mg. $OH^{\bullet}$ was captured by DMPO in water and $O_2^{\bullet-}$ was captured by DMPO in methanol. The UV and visible light were at 320–400 nm and 420–800 nm, respectively.

2.4. Photocatalytic Degradation of MB. Stirred batch experiments of MB degradation were performed using TiO_2, B-TiO_2, N-TiO_2, B/N-TiO_2, Fe-TiO_2, B-Fe-TiO_2, N/Fe-TiO_2, and B-N/Fe-TiO_2. UV light irradiation and visible light irradiation were achieved using a 250 W high-pressure Hg lamp and xenon lamp with UV cut-off filter, respectively. Under the UV or visible light irradiation conditions, the lamp was hanged in a dark box and kept at about 20 cm above the reacting liquid.

Stirred batch experiments were conducted in 10 mg/L MB solution with 1 g/L catalyst compositions added. Prior to irradiation, the solution with suspending catalyst composites was

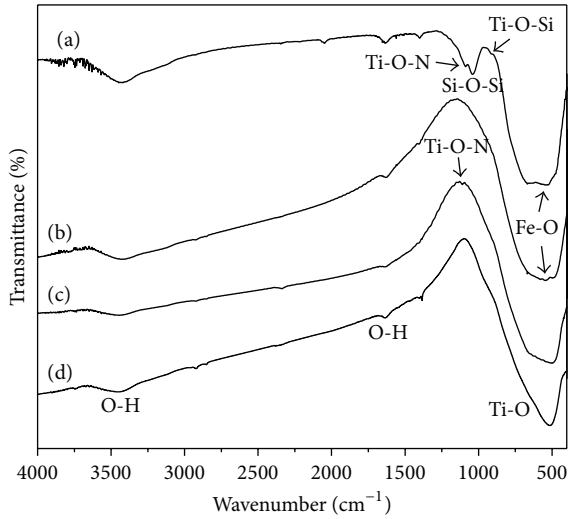

Figure 1: FTIR spectra of different catalysts: (a) B-N/Fe-TiO_2, (b) Fe-TiO_2, (c) N-TiO_2, and (d) TiO_2.

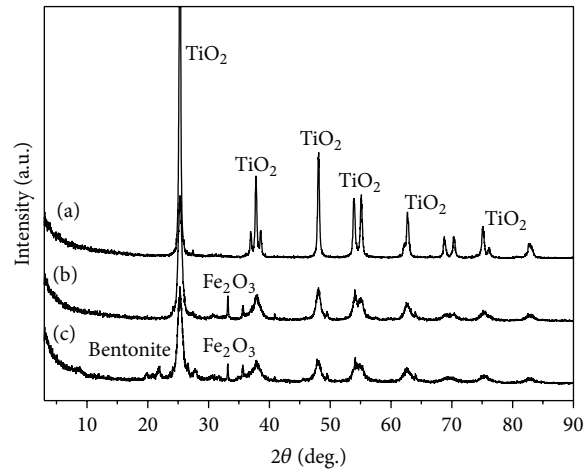

Figure 2: XRD spectra of different catalysts: (a) TiO_2, (b) N/Fe-TiO_2, and (c) B-N/Fe-TiO_2.

stirred in dark for 30 min to attain the adsorption-desorption equilibrium for MB and dissolved oxygen (DO) on the surface of the catalyst composites. Then, with continuous stirring, the solutions were illuminated with UV for 120 minutes or visible light for 200 minutes. During the degradation reactions, at given time intervals, 2 mL solution containing suspensions were sampled from the batch and were filtered through a Millipore filter (pore size, 0.22 μm) immediately to separate the catalyst compositions from the solution. Finally, the residual MB concentrations in solution were determined by a UV-Vis spectrometer (Shimadzu UV-1750).

3. Results and Discussion

3.1. Characterization of Successfully Synthesized B-N/Fe-TiO_2. In order to prove that the synthesized catalysts have been successfully modified with N/Fe doping and loaded on bentonite, multiple characterization techniques were employed, including FTIR, XRD, SEM-EDS, and XRF. First, FTIR analysis in the range of 4000 cm^{-1} to 400 cm^{-1} was performed on TiO_2, N-TiO_2, Fe-TiO_2, and B-N/Fe-TiO_2 (Figure 1). As shown in Figure 1(a), for B-N/Fe-TiO_2, it has absorption peaks at 3442 cm^{-1}, 1630 cm^{-1}, 1088 cm^{-1}, 1040 cm^{-1}, 930 cm^{-1}, and 542 cm^{-1}. The absorption peaks at 3442 cm^{-1} and 1630 cm^{-1} (Figure 1(a)) were, respectively, assigned to the stretching vibration and the bending vibration of OH, due to the adsorbed water in the samples surface [32, 33]. The high adsorption at 1040 cm^{-1} was attributed to the asymmetric stretching of Si-O-Si bonds (Figure 1(a)) [7, 34], which belongs to SiO_2 as the main composition of bentonite, indicating that the catalysts have been successfully loaded on bentonite. The absorption band at 400 cm^{-1}–600 cm^{-1} was attributed to the stretching vibration of Ti-O bond [33, 35]. The adsorption at 930 cm^{-1} was attributed to Ti-O-Si which formed during calcining process [36, 37]. The absorption peak at about 1088 cm^{-1} was attributed to Ti-O-N [38], indicating the successful doping of the catalyst with N. Finally, the peak at 542 cm^{-1} was attributed to Fe-O [34, 39, 40], indicating the successful doping of the catalyst with Fe (i.e., successful substitution of Fe atom with Ti). While no absorption peak for Fe-N was observed, indicating that at sites where nitrogen atoms substitute oxygen atoms, Fe would not substitute the Ti bonded to nitrogen.

XRD measurements of TiO_2, N/Fe-TiO_2, and B-N/Fe-TiO_2 were also conducted (Figure 2). For B-N/Fe-TiO_2 (Figure 2(c)), XRD diffraction peaks at $2\theta = 25.3^\circ$, 38.6°, 48.0°, 53.9°, and 55.1° were measured, which reflected the anatase TiO_2 (101), (112), (200), (105), and (211) planes, respectively [5]. The XRD patterns indicated that pure anatase phase was synthesized using the sol-gel method in this study. Compared with N/Fe-TiO_2, B-N/Fe-TiO_2 showed additional small peaks around $2\theta = 25^\circ$, which is consistent with the characteristic diffraction peaks of bentonite (Figure 2(c)). The XRD patterns indicated the successful loading of the modified TiO_2 catalyst on bentonite. Furthermore, for pure TiO_2 photocatalyst, the characteristic diffraction peaks of TiO_2 were very sharp (Figure 2(a)), indicating that the synthesized TiO_2 was well crystallized, while, for the modified catalyst compositions of N/Fe-TiO_2 and B-N/Fe-TiO_2 (Figures 2(b) and 2(c)), the characteristic diffraction peaks of TiO_2 were much broader and the peak intensities were much lower. Such peak broadening indicated the successful doping of N and Fe: due to different radii of N and O, Fe and Ti, doping TiO_2 with N (i.e., nitrogen atoms substitute oxygen sites in TiO_2) or Fe (i.e., Fe can enter TiO_2 lattice by substituting Ti) can lead to TiO_2 lattice distortion, resulting in the observed broadening of the TiO_2 diffraction peaks [41–43]. According to Scherrer formula calculation [7, 44], the average particle sizes of TiO_2, N/Fe-TiO_2, and B-N/Fe-TiO_2 were around 25.1 nm, 11.2 nm, and 9.5 nm, respectively. It indicated that N or Fe doping and bentonite loading could inhibit the growth of TiO_2. In addition, XRD pattern of B-N/Fe-TiO_2 (Figure 2(c)) showed the characteristic peaks of Fe_2O_3. It is possible that Fe_2O_3 were generated during calcination of Fe^{3+} doped TiO_2 gel.

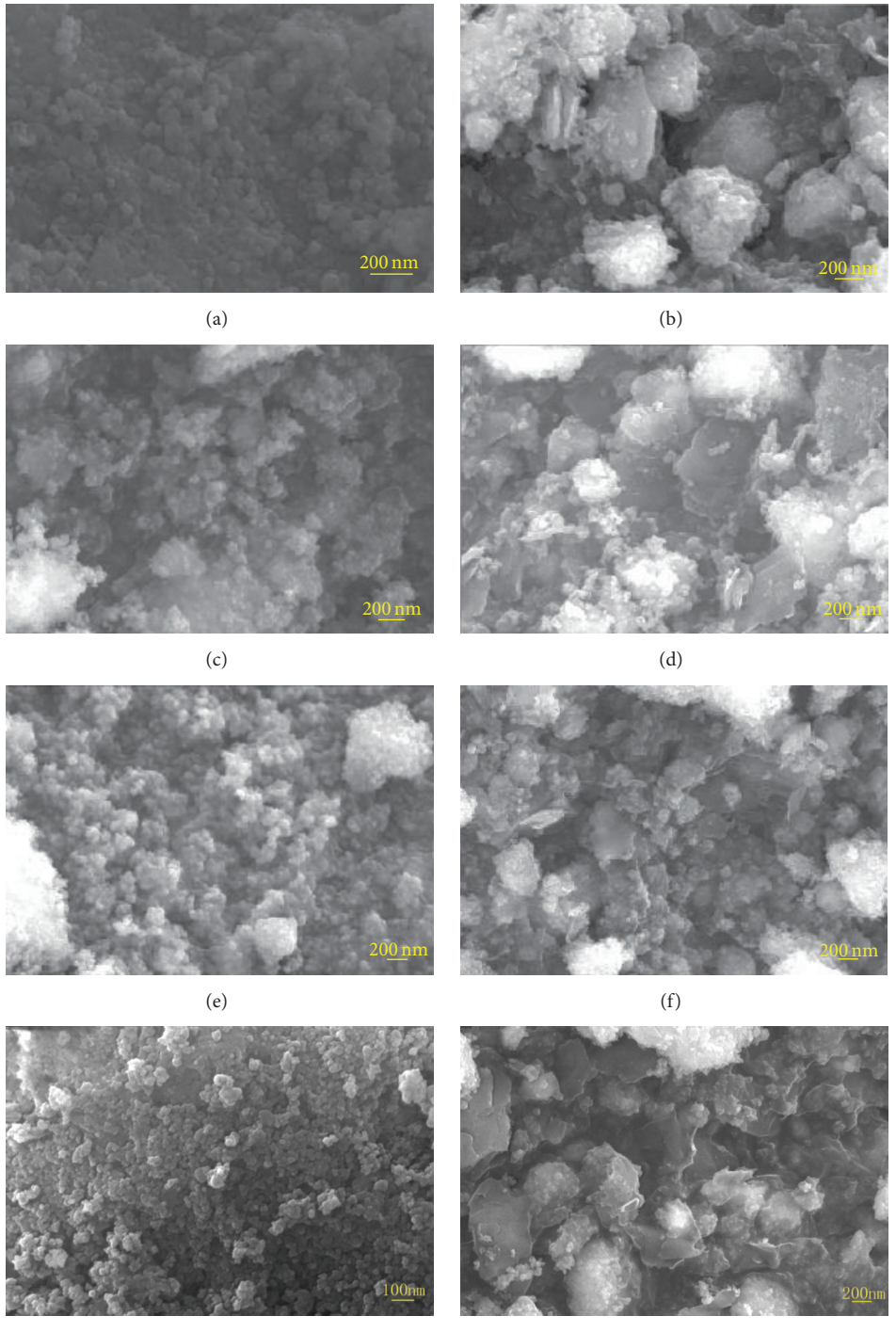

Figure 3: SEM images of synthesized catalyst composites (a) TiO_2, (b) B-TiO_2, (c) N-TiO_2, (d) B-N-TiO_2, (e) Fe-TiO_2, (f) B- Fe-TiO_2, (g) N/Fe-TiO_2, and (h) B-N/Fe-TiO_2.

Future studies of the potential calcination effect on Fe_2O_3 formation can be performed; however, it is not the focus of the present study.

To further confirm the successful doping of N and Fe in TiO_2 and their loading onto bentonite, the morphologies of the modified catalyst composites were observed by SEM (Figure 3), and the elemental compositions of the synthesized B-N/Fe-TiO_2 catalyst composites were also measured by EDS (Figure 4). In the absence of bentonite, the catalysts nanoparticles of TiO_2, N-TiO_2, Fe-TiO_2, and N/Fe-TiO_2 tended to aggregation, whereas, for synthesized B-TiO_2, B-N-TiO_2, B-Fe-TiO_2, and B-N/Fe-TiO_2, TiO_2 nanoparticles

Table 1: Specific surface areas and TiO_2 weight percentages (wt%) of the catalyst composites.

Catalysts	P25	TiO_2	B-TiO_2	N-TiO_2	Fe-TiO_2	N/Fe-TiO_2	B-N-TiO_2	B-Fe-TiO_2	B-N/Fe-TiO_2
Specific surface area (m^2/g)	55.25	45.01	60.91	53.14	64.17	66.04	65.99	77.23	91.60
TiO_2 wt%	100	100	85.7	99.8	91.9	92.6	86.5	82.1	84.8

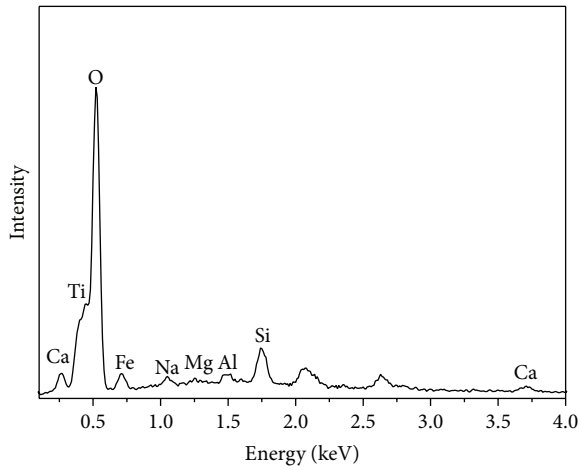

Figure 4: EDS spectra for B-N/Fe-TiO_2.

were observed to attach onto the dispersed lamellar bentonite and the aggregation was decreased in the presence of bentonite.

EDS measurement of B-N/Fe-TiO_2 (Figure 4) showed the presence of Ti, confirming the loading of TiO_2 in the catalyst composite. Also, the presence of Si, Al, Na, Ca, and Mg elements indicated the presence of Na-bentonite in the synthesized B-N/Fe-TiO_2 catalyst composite. Moreover, the presence of Fe elements demonstrated the successful doping of Fe.

In addition, the weight percentages of TiO_2 in different catalyst composites were quantified using XRF. As shown in Table 1, the weight percentages of TiO_2 in N-TiO_2, Fe-TiO_2, and N/Fe-TiO_2 were 99.8%, 91.9%, and 92.6%, respectively. The results showed that N doping contributed to only 0.2% weight of the catalyst composites, which was consistent with the fact that N in the composites was below the detection limit of EDS, while Fe_2O_3 which formed in Fe^{3+} doping contributed to ~5.5–8% of the total weight. For the catalysts loaded on bentonite, the weight percentages of TiO_2 in the catalyst composites were much lower, being 85.7%, 86.5%, 82.1%, and 84.8% for B-TiO_2, B-N-TiO_2, B-Fe-TiO_2, and B-N/Fe-TiO_2, respectively, indicating that bentonite contributed to ~9–14% of total weight of the catalyst composites.

In summary, FTIR, XRD, SEM-EDS, and XRF were employed to characterize the newly synthesized B-N/Fe-TiO_2 catalyst composites, and consistent results were obtained. All measurements confirmed the successful N/Fe doping in TiO_2 and their successful loading onto bentonite. Very small amount of N (0.2% weight) was doped in the catalyst, and Fe doping (~7-8%) and bentonite loading (~8–14%) contributed significantly to the total mass of the catalyst composites.

3.2. Highest Specific Surface Area of Newly Synthesized B-N/Fe-TiO_2. As specific surface area is an important parameter determining the reactivity of catalyst, here, the specific surface area of the synthesized TiO_2 catalyst composites was measured (Table 1). First, the effects of N and/or Fe doping on the specific surface area of the catalyst composites were investigated. As shown in Table 1, the specific surface areas of TiO_2, N-TiO_2, Fe-TiO_2, and N/Fe-TiO_2 were 45.01, 53.13, 64.17, and 66.04 m^2/g, respectively. The results showed that doping N and Fe slightly increased the specific surface area of TiO_2 catalyst composite. As discussed in Section 3.1, N and/or Fe doping in TiO_2 can lower the crystallinity of the TiO_2, which may result in more specific surface area available for N_2 adsorption.

Also, the effects of bentonite loading on the specific surface area of the catalyst composites were investigated. The specific surface areas of B-TiO_2, B-N-TiO_2, B-Fe-TiO_2, and B-N/Fe-TiO_2 were 60.91, 65.99, 77.23, and 91.60 m^2/g, respectively. The measurements showed that the presence of bentonite dramatically increased the specific surface area of the TiO_2 catalyst composites. Since natural bentonite has lamellar structure, it has large interlayer surface area for TiO_2 attachment. The TiO_2 attached onto bentonite particles can be stabilized on bentonite surfaces, which can avoid the aggregation of TiO_2 nanoparticles.

3.3. Highest UV-Vis Light Absorption of Synthesized B-N/Fe-TiO_2. Generally in natural photodegradation processes photocatalyst can absorb the ultraviolet (UV) and/or visible light from natural sunlight and utilize the energy for the redox degradation reactions. To characterize the absorption of UV and visible light by the synthesized TiO_2 composites, UV-Vis diffuse reflectance spectra of the photocatalyst composites TiO_2, P25, N-TiO_2, Fe-TiO_2, B-TiO_2, B-N-TiO_2, B-Fe-TiO_2, N/Fe-TiO_2, and B-N/Fe-TiO_2 were measured (Figure 5). For synthesized TiO_2 (Figure 5(i)) and the purchased P25 type TiO_2 (Figure 5(h)), significant absorption was observed for light with wavelength shorter than 390 nm. This is the intrinsic absorption edge of TiO_2 for the electron transfer from O_{2p} to Ti_{3d}, corresponding with the valence band to conduction band transition of TiO_2 [7, 45]. For these TiO_2 composites without Fe and/or N doping, there was almost no light absorption in the visible light region, with wavelength ranging from 400 to 800 nm.

Since bentonite can absorb visible light, B-TiO_2 had more absorption of visible light than bare TiO_2. For TiO_2 composites doped with Fe^{3+} (Figures 5(a), 5(b), 5(c), and 5(d)), they showed significant enhancement in visible light absorption. This is because Fe^{3+} doping or Fe_2O_3 could form a dopant energy level within the band gap of TiO_2. It was studied that Fe_2O_3 has small band gap (E_g = 2.1 ev)

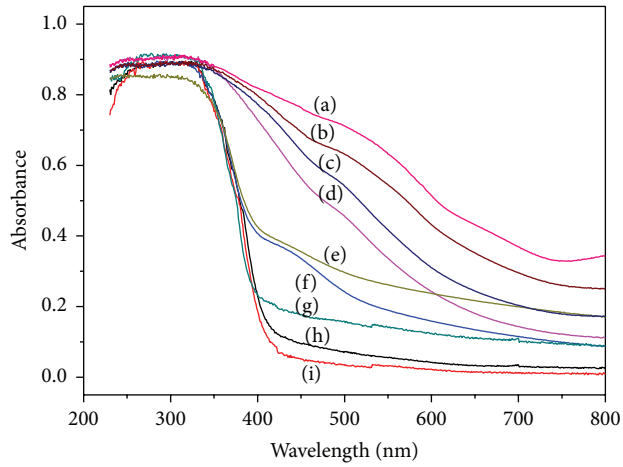

(a) B-N/Fe-TiO_2
(b) N/Fe-TiO_2
(c) B-Fe-TiO_2
(d) Fe-TiO_2
(e) B-N-TiO_2
(f) N-TiO_2
(g) B-TiO_2
(h) P25
(i) TiO_2

Figure 5: UV-Vis diffuse reflection spectra of different catalysts.

and can absorb and utilize about 40% of the incident solar spectra [46]. N doping (Figures 5(a), 5(b), 5(e), and 5(f)) also increased the adsorption in visible light region. Our observation here was consistent with previous studies, which showed that N doping into the lattice of TiO_2 can shift the absorption edge of TiO_2 into the visible light range and exhibit increased absorption between 400 nm and 600 nm [47]. This is because nitrogen doping can form the localized midgap states above the top of the valence band of TiO_2 reducing the band gap of TiO_2. To further conform the N or Fe doping effects, the formula $E_g = 1240/\lambda_g$ (where E_g is the band gap and λ_g is the absorption edge shown in Figure 5) was used to calculate the catalyst's band gap. The band gaps of TiO_2, N-TiO_2, Fe-TiO_2, N/Fe-TiO_2, and B-N/Fe-TiO_2 were calculated to be 3.26, 2.95, 2.34, 2.17, and 2.03 eV, respectively. The results showed that B-N/Fe-TiO_2 had the smallest band gap and its electrons could be easily excited from the valence band to the conduction band under visible light irradiation.

In conclusion, N and/or Fe doping reduced the band gap of the TiO_2 catalyst composites, therefore extending the light absorption of the modified catalysts from UV to the visible light region. In addition, the comodification with N and Fe showed synergistic effect in reducing the band gap of the TiO_2 catalyst composites. Meanwhile, bentonite can absorb visible light as well. Therefore, compared with all TiO_2 catalyst composites (Figure 5), the newly synthesized B-N/Fe-TiO_2 (Figure 5(a)) showed the highest light absorption in the UV-Vis region.

3.4. $OH^\bullet$ and $O_2^{\bullet-}$ Generation under UV-Vis. As hydroxyl radicals $OH^\bullet$ and super oxygen ions $O_2^{\bullet-}$ play key roles in the pollutant degradation process, the generation of free radicals ($OH^\bullet$ and $O_2^{\bullet-}$) during photoirradiation process (shown in (1)–(3)) was investigated. The EPR spectra of the same weight of pure TiO_2, N/Fe-TiO_2, and B-N/Fe-TiO_2 with UV (Figure 6) and visible irradiation (Figure 7) were obtained. The intensity of the signal represented the relative amount of $OH^\bullet$ and $O_2^{\bullet-}$ produced by the photocatalyst. The constants of $OH^\bullet$ were $g = 2.005$, $a_N = a_H = 1.49$ mT, and the constants of $O_2^{\bullet-}$ were $g = 2.002$, $a_N = 1.27$ mT, $a_H{}^\beta = 1.026$ mT, and $a_H{}^\gamma = 0.187$ mT.

$$TiO_2 + h\nu \longrightarrow e_{CB} + h_{VB} \quad (1)$$

$$OH^- + h_{VB} \longrightarrow OH^\bullet \quad (2)$$

$$O_2 + e_{CB} \longrightarrow O_2^{\bullet-} \quad (3)$$

Compared with TiO_2 system, the radicals of $OH^\bullet$ and $O_2^{\bullet-}$ in modified TiO_2 were significantly generated under UV-Vis light. Under UV irradiation, the intensities of $OH^\bullet$ and $O_2^{\bullet-}$ were about 1810 and 380 in N/Fe-TiO_2 system, respectively, while $OH^\bullet$ and $O_2^{\bullet-}$ in B-N/Fe-TiO_2 system were about 1740 and 460, respectively. The amount of $OH^\bullet$ produced by N/Fe-TiO_2 was slightly higher than that produced by B-N/Fe-TiO_2, while the amount of $O_2^{\bullet-}$ produced by N/Fe-TiO_2 was slightly lower than the later one. As the strong cations exchange ability of bentonite, the surface of B-N/Fe-TiO_2 had more electrons which can produce more $O_2^{\bullet-}$. Under visible irradiation, the amounts of $OH^\bullet$ and $O_2^{\bullet-}$ generated by N/Fe-TiO_2 were about 830 and 180; the amount of $OH^\bullet$ and $O_2^{\bullet-}$ generated by B-N/Fe-TiO_2 were about 880 and 260, respectively. The free radicals produced by B-N/Fe-TiO_2 were both higher than N/Fe-TiO_2 under visible light. It resulted from the highest visible light absorption of B-N/Fe-TiO_2, and it could form more electron-hole pairs and more free radicals in visible region.

3.5. Highest MB Photodegradation Efficiency of Synthesized B-N/Fe-TiO_2. To compare the photocatalytic efficiency of

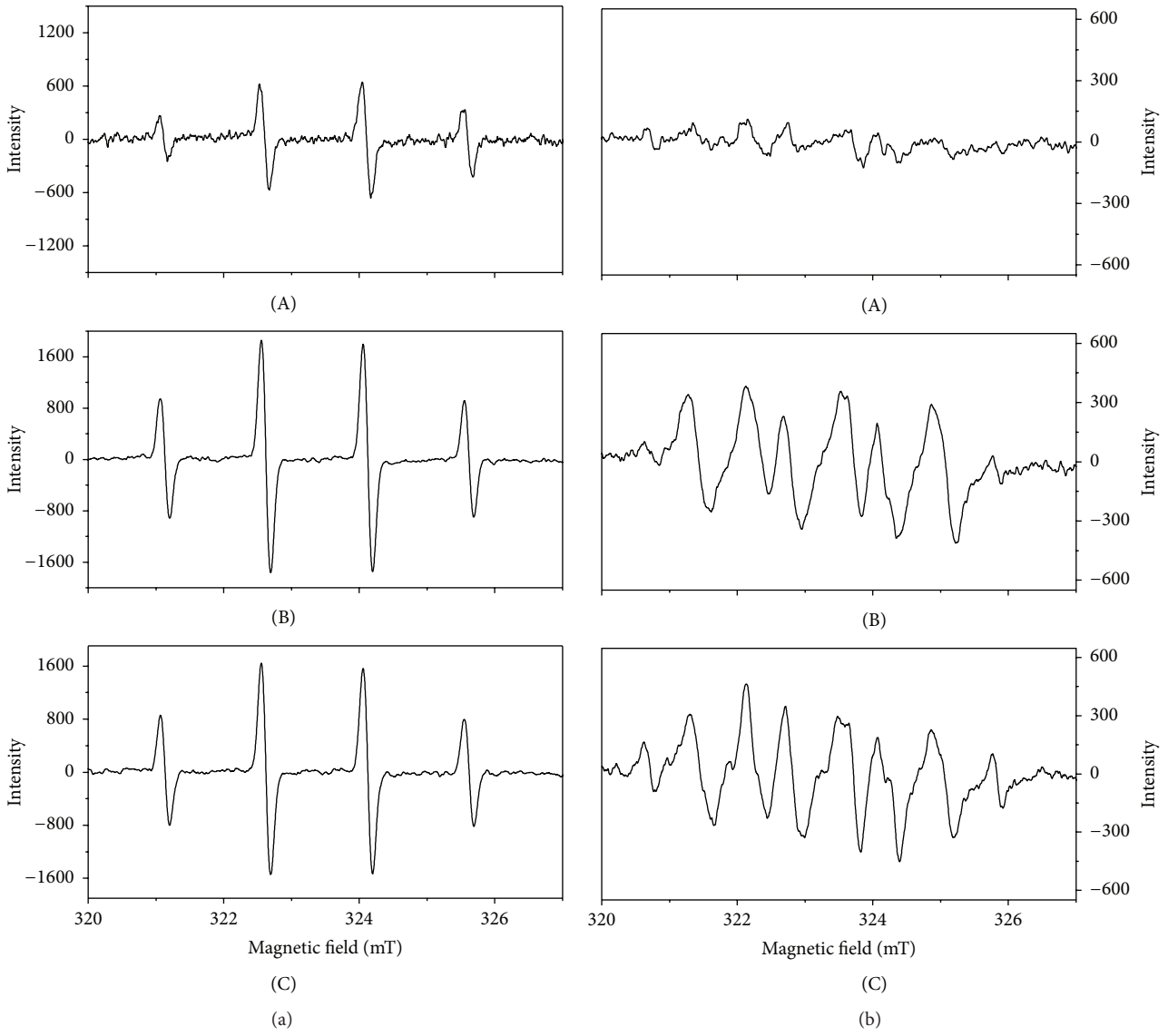

Figure 6: EPR spectra of the $OH^{\bullet}$ (a) and $O_2^{\bullet-}$ (b) radicals formed upon UV irradiation with catalysts: (A) TiO_2, (B) N/Fe-TiO_2, and (C) B-N/Fe-TiO_2.

different catalyst composites, the degradation of MB was conducted with the addition of 1 g/L of different catalyst composites (bentonite, TiO_2, B-TiO_2, N-TiO_2, Fe-TiO_2, N/Fe-TiO_2, B-N-TiO_2, B-Fe-TiO_2, and B-N/Fe-TiO_2). The residual MB concentrations in solution after reaction under UV (Figure 8(a)) and visible light irradiation (Figure 8(b)) for different time intervals were measured. Figure 8 showed that bentonite has slight influence on the degradation of MB. Without catalyst TiO_2, MB did not degrade under UV and visible light. With the addition of different catalyst composites, various degradation kinetics were observed (Figure 8). Under UV light irradiation, B-N/Fe-TiO_2 showed the highest photocatalytic activity for MB degradation with 100% MB removal in 50 minutes. For N/Fe-TiO_2, the slower process with 100% MB removal was used in 80 minutes. The photocatalytic efficiency of MB removal by TiO_2, B-TiO_2, N-TiO_2, Fe-TiO_2, B-N-TiO_2, and B-Fe-TiO_2 within 120 minutes was 56.7%, 45.1%, 94.7%, 69.2%, 89.2%, and 76.5%, respectively. Comparably, under visible light, B-N/Fe-TiO_2 also performed the fastest degradation of 100% MB in 180 minutes. The rates of MB degradation by TiO_2, B-TiO_2, N-TiO_2, Fe-TiO_2, B-N-TiO_2, B-Fe-TiO_2, and N/Fe-TiO_2 were 15.2%, 19.1%, 31.1%, 37.8%, 27.8%, 41.8%, and 85.5%, respectively. The results indicated that the newly synthesized B-N/Fe-TiO_2 showed the fastest photocatalyst efficiency for MB degradation under both UV and visible lights. As discussed earlier, B-N/Fe-TiO_2 had the highest specific surface area and the highest UV-Vis adsorption, both of which can contribute to its fastest photocatalyst efficiency for MB degradation.

The photocatalytic efficiency improvement for the B-N/Fe-TiO_2 compared to N/Fe-TiO_2 under visible light (Figure 8(b)) was more significant than under UV light

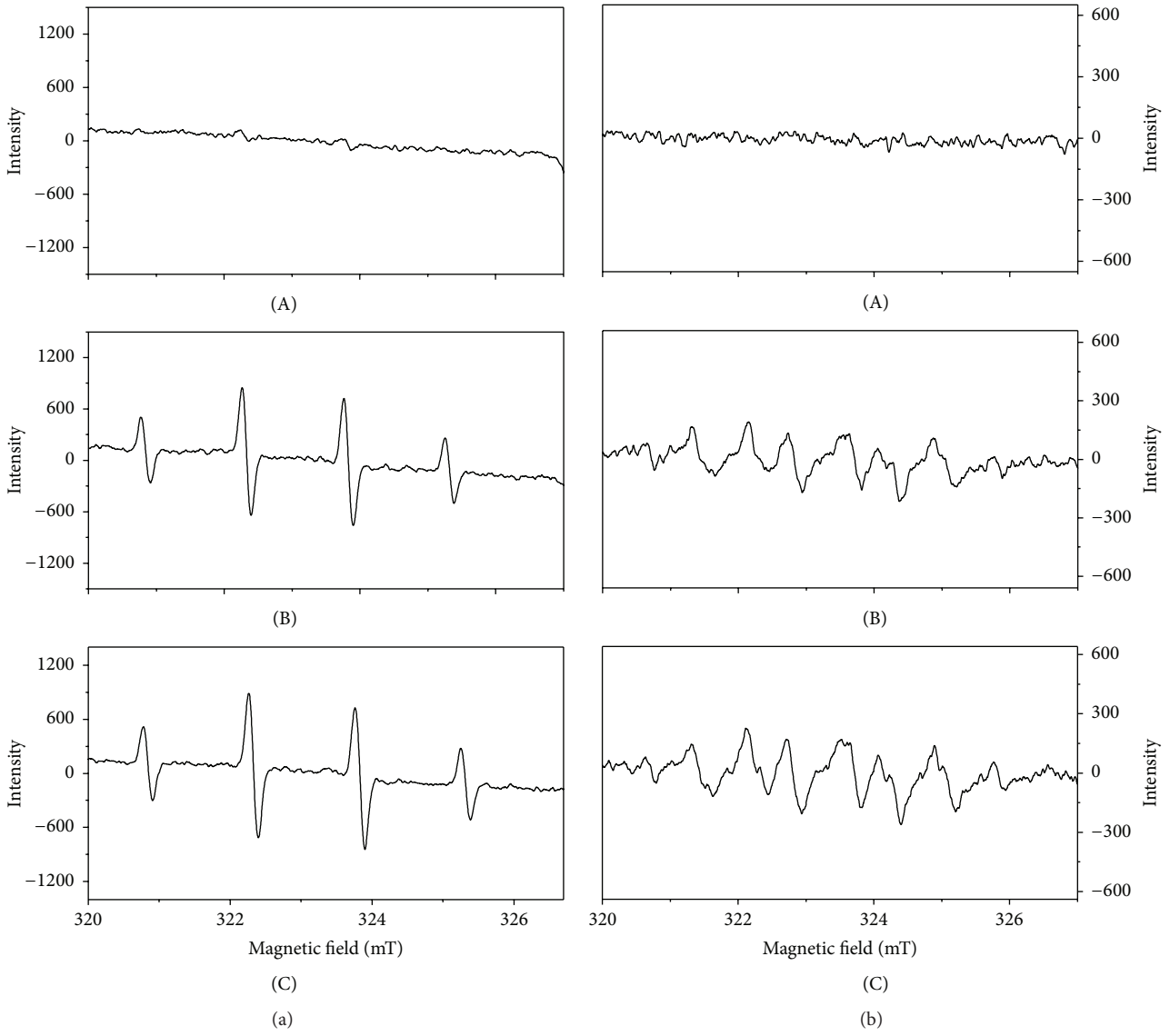

Figure 7: EPR spectra of the $OH^{\bullet}$ (a) and $O_2^{\bullet-}$ (b) radicals formed upon visible irradiation with catalysts: (A) TiO_2, (B) N/Fe-TiO_2, and (C) B-N/Fe-TiO_2.

(Figure 8(a)) irradiation. This is because bentonite can adsorb visible light and B-N/Fe-TiO_2 can produce more free radicals under visible light. In terms of energy, sunlight at Earth's surface is about 52–55% infrared, 42-43% visible, and 3–5% UV. Considering the much smaller energy percentage of UV (3–5%) than visible light (42-43%) on Earth's surface, the newly synthesized B-N/Fe-TiO_2 is going to significantly increase the photocatalytic efficiency of the catalyst using sunlight.

4. Conclusion

In this study, bentonite supported (N/Fe) comodified TiO_2 nanoparticles composite (B-N/Fe-TiO_2) was successfully synthesized by sol-gel method. The novel photocatalyst B-N/Fe-TiO_2 could extend the UV-Vis light working range and enhance the degradation of MB in water. B-N/Fe-TiO_2 enhanced photoactivity attributes to its larger surface area and higher UV and visible light adsorption. In particular, the newly synthesized B-N/Fe-TiO_2 showed significantly increased photocatalytic efficiency for contaminant degradation under visible light, making it a good photocatalyst for water remediation under sunlight.

Conflict of Interests

The authors declare that there is no conflict of interests regarding the publication of this paper.

Acknowledgments

This study was supported by National Natural Science Foundation of China (41472232, 41272061), Fundamental Research

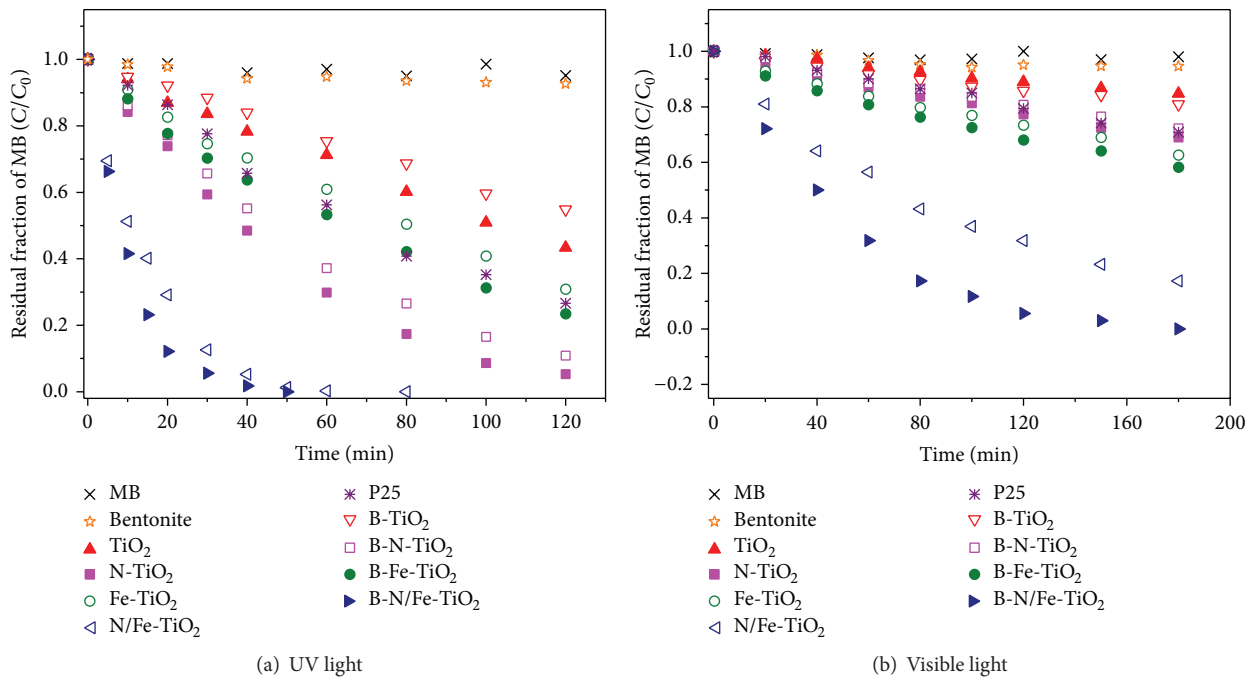

FIGURE 8: Residual concentrations of MB in solution after reaction for different time intervals and in the absence and the presence of TiO_2, B-TiO_2, N-TiO_2, Fe-TiO_2, N/Fe-TiO_2, B-N-TiO_2, B-Fe-TiO_2, and B-N/Fe-TiO_2 under UV (a) and visible (b) light irradiation.

Funds for the Central Universities, Open Program of State Key Laboratory of Biogeology and Environmental Geology (GBL21404), and Prospective Basic Research Project of China Waterborne Transport Research Institute (WTI61421).

References

[1] K. Yu, L. Huang, L.-L. Lou et al., "Degradation of polycyclic aromatic hydrocarbons in crumb tyre rubber catalysed by rutile TiO_2 under UV irradiation," *Environmental Technology*, vol. 36, no. 8, pp. 1008–1015, 2015.

[2] Z. Huang, P.-C. Maness, D. M. Blake, E. J. Wolfrum, S. L. Smolinski, and W. A. Jacoby, "Bactericidal mode of titanium dioxide photocatalysis," *Journal of Photochemistry and Photobiology A: Chemistry*, vol. 130, no. 2-3, pp. 163–170, 2000.

[3] M. Pelaez, P. Falaras, A. G. Kontos et al., "A comparative study on the removal of cylindrospermopsin and microcystins from water with NF-TiO_2-P25 composite films with visible and UV-vis light photocatalytic activity," *Applied Catalysis B: Environmental*, vol. 121-122, pp. 30–39, 2012.

[4] N. De la Cruz, R. F. Dantas, J. Giménez, and S. Esplugas, "Photolysis and TiO_2 photocatalysis of the pharmaceutical propranolol: solar and artificial light," *Applied Catalysis B: Environmental*, vol. 130, pp. 249–256, 2013.

[5] J. Y. Li, Y. Su, and W. B. Wang, "A study of photodegradation of sulforhodamine B on Au-TiO_2/bentonite under UV and visible light irradiation," *Solid State Science*, vol. 11, no. 12, pp. 2037–2043, 2009.

[6] W. Qian, P. A. Greaney, S. Fowler, S.-K. Chiu, A. M. Goforth, and J. Jiao, "Low-temperature nitrogen doping in ammonia solution for production of N-Doped TiO_2-hybridized graphene as a highly efficient photocatalyst for water treatment," *ACS Sustainable Chemistry & Engineering*, vol. 2, no. 7, pp. 1802–1810, 2014.

[7] E. Rossetto, D. I. Petkowicz, J. H. Z. dos Santos, S. B. C. Pergher, and F. G. Penha, "Bentonites impregnated with TiO_2 for photodegradation of methylene blue," *Applied Clay Science*, vol. 48, no. 4, pp. 602–606, 2010.

[8] S. Thiripuranthagan, D. Raj, and K. Kannan, "Photocatalytic degradation of congored on silica supported Ag impregnated TiO_2," *Journal of Nanoscience and Nanotechnology*, vol. 15, no. 6, pp. 4727–4733, 2015.

[9] X. F. Yang, J. L. Qin, Y. Jiang et al., "Fabrication of P25/Ag_3PO_4/graphene oxide heterostructures for enhanced solar photocatalytic degradation of organic pollutants and bacteria," *Applied Catalysis B: Environmental*, vol. 166-167, pp. 231–240, 2015.

[10] M. M. Dávila-Jiménez, M. P. Elizalde-González, E. García-Díaz, V. Marín-Cevada, and J. Zequineli-Pérez, "Photodegradation of the anthraquinonic dye acid Green 25 by TiO_2 immobilized on carbonized avocado kernels: intermediates and toxicity," *Applied Catalysis B: Environmental*, vol. 166, pp. 241–250, 2015.

[11] L.-L. Tan, W.-J. Ong, S.-P. Chai, and A. R. Mohamed, "Noble metal modified reduced graphene oxide/TiO_2 ternary nanostructures for efficient visible-light-driven photoreduction of carbon dioxide into methane," *Applied Catalysis B: Environmental*, vol. 166-167, pp. 251–259, 2015.

[12] X. Bu, Y. Wang, J. Li, and C. Zhang, "Improving the visible light photocatalytic activity of TiO_2 by combining sulfur doping and rectorite carrier," *Journal of Alloys and Compounds*, vol. 628, pp. 20–26, 2015.

[13] M. Shahid, I. El Saliby, L. D. Tijing et al., "Synthesis and characterisation of silica-modified titania for photocatalytic decolouration of crystal violet," *Journal of Nanoscience and Nanotechnology*, vol. 15, no. 7, pp. 5326–5329, 2015.

[14] R. Asahi, T. Morikawa, T. Ohwaki, K. Aoki, and Y. Taga, "Visible-light photocatalysis in nitrogen-doped titanium oxides," *Science*, vol. 293, no. 5528, pp. 269–271, 2001.

[15] J. Zhang, Y. M. Wu, M. Y. Xing, S. A. K. Leghari, and S. Sajjad, "Development of modified N doped TiO_2 photocatalyst with metals, nonmetals and metal oxides," *Energy and Environmental Science*, vol. 3, no. 6, pp. 715–726, 2010.

[16] J. Ananpattarachai, P. Kajitvichyanukul, and S. Seraphin, "Visible light absorption ability and photocatalytic oxidation activity of various interstitial N-doped TiO_2 prepared from different nitrogen dopants," *Journal of Hazardous Materials*, vol. 168, no. 1, pp. 253–261, 2009.

[17] G. Halasi, G. Schubert, and F. Solymosi, "Comparative study on the photocatalytic decomposition of methanol on TiO_2 modified by N and promoted by metals," *Journal of Catalysis*, vol. 294, pp. 199–206, 2012.

[18] M. Batzill, E. H. Morales, and U. Diebold, "Influence of nitrogen doping on the defect formation and surface properties of TiO_2 rutile and anatase," *Physical Review Letters*, vol. 96, Article ID 026103, 2006.

[19] P. Goswami and J. N. Ganguli, "Evaluating the potential of a new titania precursor for the synthesis of mesoporous Fe-doped titania with enhanced photocatalytic activity," *Materials Research Bulletin*, vol. 47, no. 8, pp. 2077–2084, 2012.

[20] H.-J. Lin, T.-S. Yang, M.-C. Wang, and C.-S. Hsi, "Structural and photodegradation behaviors of $Fe3^+$-doping TiO_2 thin films prepared by a sol-gel spin coating," *Journal of Alloys and Compounds*, vol. 610, pp. 478–485, 2014.

[21] Z. J. Li, W. Z. Shen, W. S. He, and X. T. Zu, "Effect of Fe-doped TiO_2 nanoparticle derived from modified hydrothermal process on the photocatalytic degradation performance on methylene blue," *Journal of Hazardous Materials*, vol. 155, no. 3, pp. 590–594, 2008.

[22] X. Z. Yang, H. Y. Zhu, J. W. Liu et al., "A mesoporous structure for efficient photocatalysts: anatase nanocrystals attached to leached clay layers," *Microporous and Mesoporous Materials*, vol. 112, no. 1–3, pp. 32–44, 2008.

[23] L. V. Barbosa, L. Marçal, E. J. Nassar et al., "Kaolinite-titanium oxide nanocomposites prepared via sol-gel as heterogeneous photocatalysts for dyes degradation," *Catalysis Today*, vol. 246, pp. 133–142, 2015.

[24] J. Ménesi, L. Körösi, É. Bazsó, V. Zöllmer, A. Richardt, and I. Dékány, "Photocatalytic oxidation of organic pollutants on titania–clay composites," *Chemosphere*, vol. 70, no. 3, pp. 538–542, 2008.

[25] J. J. Liu, M. Q. Dong, S. L. Zuo, and Y. C. Yu, "Solvothermal preparation of TiO_2/montmorillonite and photocatalytic activity," *Applied Clay Science*, vol. 43, no. 2, pp. 156–159, 2009.

[26] H. Hao and J. Zhang, "The study of Iron (III) and nitrogen co-doped mesoporous TiO_2 photocatalysts: synthesis, characterization and activity," *Microporous and Mesoporous Materials*, vol. 121, no. 1–3, pp. 52–57, 2009.

[27] Y. Cong, J. L. Zhang, F. Chen, M. Anpo, and D. N. He, "Preparation, photocatalytic activity, and mechanism of nano-TiO_2 co-doped with nitrogen and iron (III)," *Journal of Physical Chemistry C*, vol. 111, no. 28, pp. 10618–10623, 2007.

[28] D. Dolat, S. Mozia, B. Ohtani, and A. W. Morawski, "Nitrogen, iron-single modified (N-TiO_2, Fe-TiO_2) and co-modified (Fe,N-TiO_2) rutile titanium dioxide as visible-light active photocatalysts," *Chemical Engineering Journal*, vol. 225, pp. 358–364, 2013.

[29] J. Y. Feng, R. S. K. Wong, X. Hu, and P. L. Yue, "Discoloration and mineralization of Orange II by using Fe^{3+}-doped TiO_2 and bentonite clay-based Fe nanocatalysts," *Catalysis Today*, vol. 98, no. 3, pp. 441–446, 2004.

[30] Y. Q. Yang and H. J. Chen, "Microwave synthesis of bentonite loaded N/Fe co-doped TiO_2 photocatalysts," *Journal of Xinyang Normal University*, vol. 26, pp. 276–278, 2013 (Chinese).

[31] U. G. Akpan and B. H. Hameed, "The advancements in sol-gel method of doped-TiO_2 photocatalysts," *Applied Catalysis A: General*, vol. 375, no. 1, pp. 1–11, 2010.

[32] C. Yang, Y. Zhu, J. D. Wang, Z. J. Li, X. T. Su, and C. G. Niu, "Hydrothermal synthesis of TiO_2–WO_3–bentonite composites: conventional versus ultrasonic pretreatments and their adsorption of methylene blue," *Applied Clay Science*, vol. 105-106, pp. 243–251, 2015.

[33] Z. Y. Lu, F. Chen, M. He et al., "Microwave synthesis of a novel magnetic imprinted TiO_2 photocatalyst with excellent transparency for selective photodegradation of enrofloxacin hydrochloride residues solution," *Chemical Engineering Journal*, vol. 249, pp. 15–26, 2014.

[34] M. Esmaeilpour, J. Javidi, and M. Zandi, "Preparation and characterization of Fe_3O_4@SiO_2@PMA:AS an efficient and recyclable nanocatalyst for the synthesis of 1-amidoalkyl-2-naphthols," *Materials Research Bulletin*, vol. 55, pp. 78–87, 2014.

[35] T. J. Xin, M. L. Ma, H. P. Zhang et al., "A facile approach for the synthesis of magnetic separable Fe_3O_4@TiO_2, core–shell nanocomposites as highly recyclable photocatalysts," *Applied Surface Science*, vol. 288, pp. 51–59, 2014.

[36] K. Balachandran, R. Venckatesh, R. Sivaraj, K. Hemalatha, and R. Mariappan, "Enhancing power conversion efficiency of DSSC by doping SiO_2 in TiO_2 photo anodes," *Materials Science in Semiconductor Processing*, vol. 35, pp. 59–65, 2015.

[37] J. Liu, X. Li, S. Zuo, and Y. Yu, "Preparation and photocatalytic activity of silver and TiO_2 nanoparticles/montmorillonite composites," *Applied Clay Science*, vol. 37, no. 3-4, pp. 275–280, 2007.

[38] G. H. Tian, Y. J. Chen, K. Pan et al., "Efficient visible light-induced degradation of phenol on N-doped anatase TiO_2 with large surface area and high crystallinity," *Applied Surface Science*, vol. 256, no. 12, pp. 3740–3745, 2010.

[39] Y. Luo, Z. Lu, Y. Jiang et al., "Selective photodegradation of 1-methylimidazole-2-thiol by the magnetic and dual conductive imprinted photocatalysts based on TiO_2/Fe_3O_4/MWCNTs," *Chemical Engineering Journal*, vol. 240, pp. 244–252, 2014.

[40] M. H. Cao, P. F. Wang, Y. H. Ao, C. Wang, J. Hou, and J. Qian, "Photocatalytic degradation of tetrabromobisphenol a by a magnetically separable graphene-TiO_2 composite photocatalyst: mechanism and intermediates analysis," *Chemical Engineering Journal*, vol. 264, pp. 113–124, 2015.

[41] T. Z. Huang, S. Mao, J. M. Yu, Z. Wen, G. Lu, and J. Chen, "Effects of N and F doping on structure and photocatalytic properties of anatase TiO_2 nanoparticles," *RSC Advances*, vol. 3, no. 37, pp. 16657–16664, 2013.

[42] M. C. Wang, H. J. Lin, and T. S. Yang, "Characteristics and optical properties of iron ion (Fe^{3+})-doped titanium oxide thin films prepared by a sol-gel spin coating," *Journal of Alloys and Compounds*, vol. 473, no. 1-2, pp. 394–400, 2009.

[43] J. F. Zhu, W. Zheng, B. He, J. Zhang, and M. Anpo, "Characterization of Fe-TiO_2 photocatalysts synthesized by hydrothermal method and their photocatalytic reactivity for photodegradation of XRG dye diluted in water," *Journal of Molecular Catalysis A: Chemical*, vol. 216, no. 1, pp. 35–43, 2004.

[44] Q. Wang, X. Liu, X. Wei, J. Dai, and W. Li, "Ferromagnetic property of Co and Ni doped TiO_2 nanoparticles," *Journal of Nanomaterials*, vol. 2015, Article ID 371582, 5 pages, 2015.

[45] J. Liqiang, S. Xiaojun, C. Weimin, X. Zili, D. Yaoguo, and F. Honggang, "The preparation and characterization of nanoparticle TiO_2/Ti films and their photocatalytic activity," *Journal of Physics and Chemistry of Solids*, vol. 64, no. 4, pp. 615–623, 2003.

[46] J. S. Jang, K. Y. Yoon, Y. Xiao, F.-R. F. Fan, and A. J. Bard, "Development of a potential Fe_2O_3-based photocatalyst thin film for water oxidation by scanning electrochemical microscopy: effects of Ag-Fe_2O_3 nanocomposite and Sn doping," *Chemistry of Materials*, vol. 21, no. 20, pp. 4803–4810, 2009.

[47] Y. Cong, J. Zhang, F. Chen, and M. Anpo, "Synthesis and characterization of nitrogen-doped TiO_2 nanophotocatalyst with high visible light activity," *Journal of Physical Chemistry C*, vol. 111, no. 19, pp. 6976–6982, 2007.